Electronic Supplementary Information

A single bottom facet outperforms random multifacets in a nanoparticle-on-metallic-mirror system†

*Vasanthan Devaraj,[‡a] Jong-Min Lee,[‡a] Samir Adhikari,[‡b] Minjun Kim,[b] Donghan Lee[*b] and Jin-Woo Oh[*ac]*

[a]BIT Fusion Technology Center, Pusan National University, Busan, South Korea

[b]Department of Physics, Chungnam National University, Daejeon, South Korea

[c]Department of Nano Energy Engineering, Pusan National University, Busan, South Korea

‡These authors contributed equally

*Corresponding authors' emails: dleee@cnu.ac.kr, ojw@pusan.ac.kr

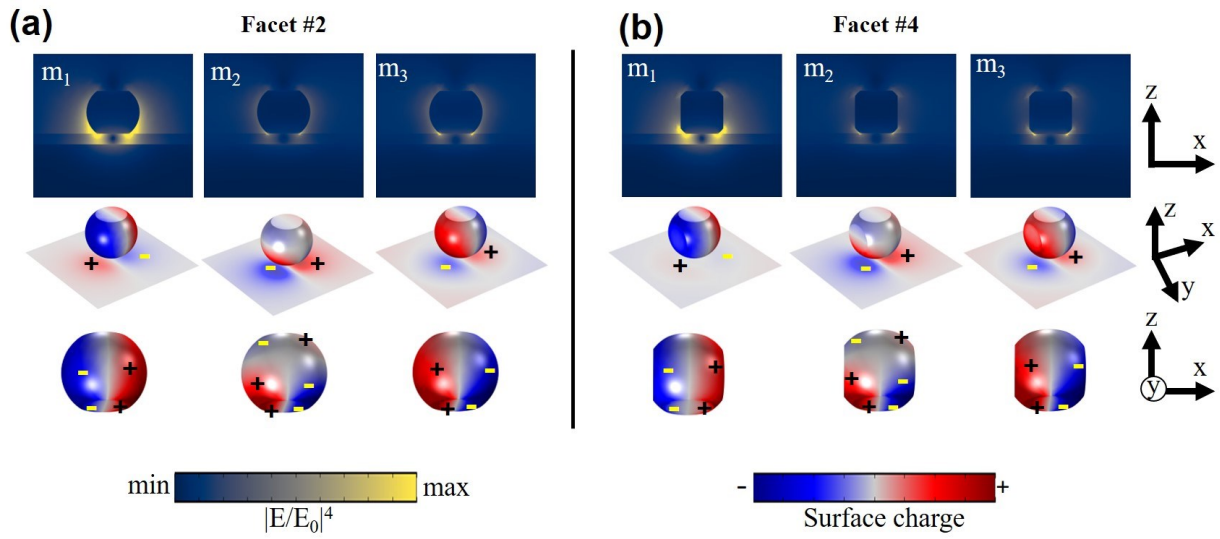

Figure S1. Cross-sectional XZ electric field amplitude profiles and 3D SCDM results for the facet #2 (a) and #4 (b) samples, based on the classification of modes (m_1 to m_3).

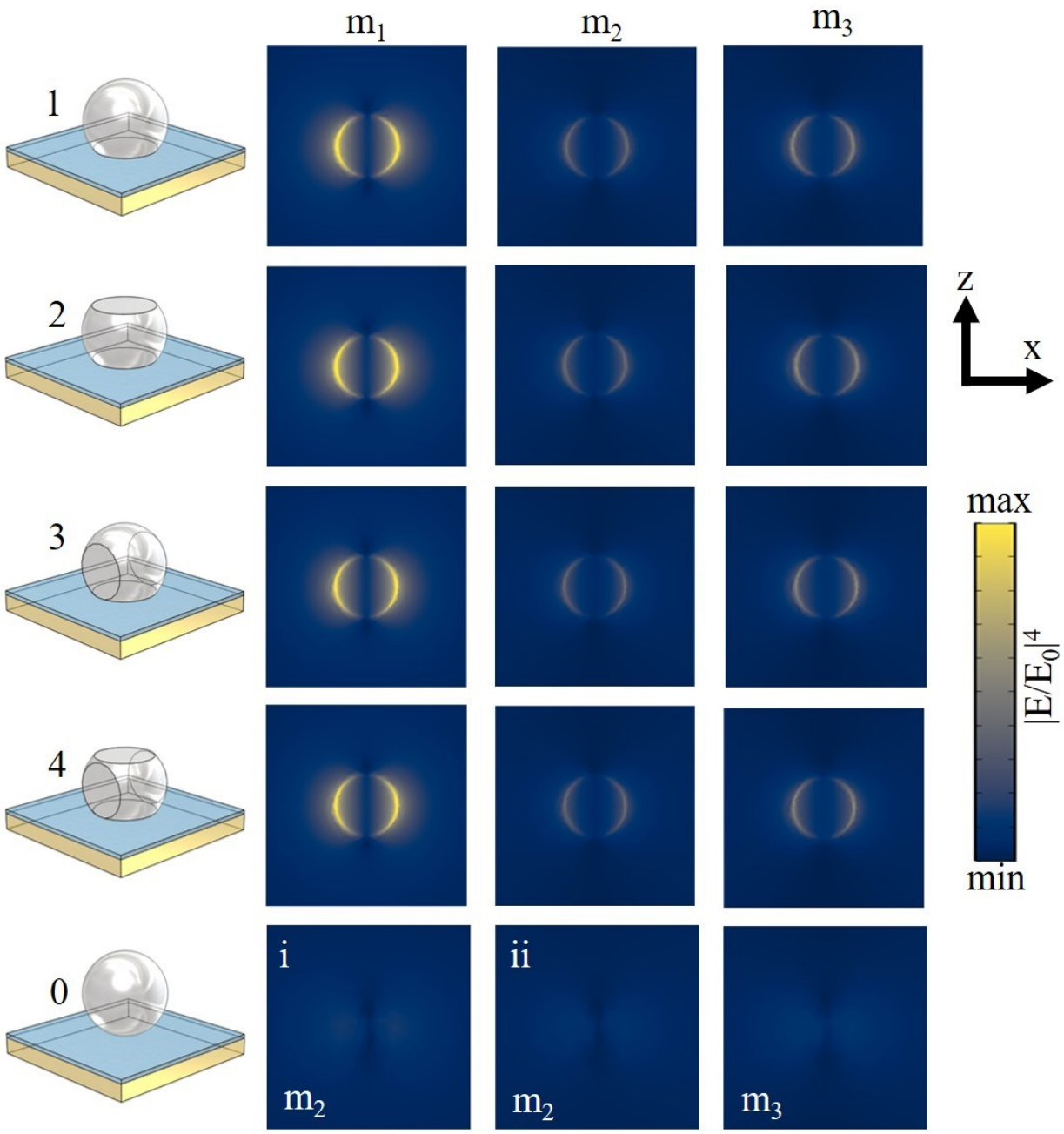

Figure S2. Cross-sectional XY electric field amplitude profiles characterizing the performances of random faceted designs in the NPOM. The gap size "g" was fixed at 20 nm.

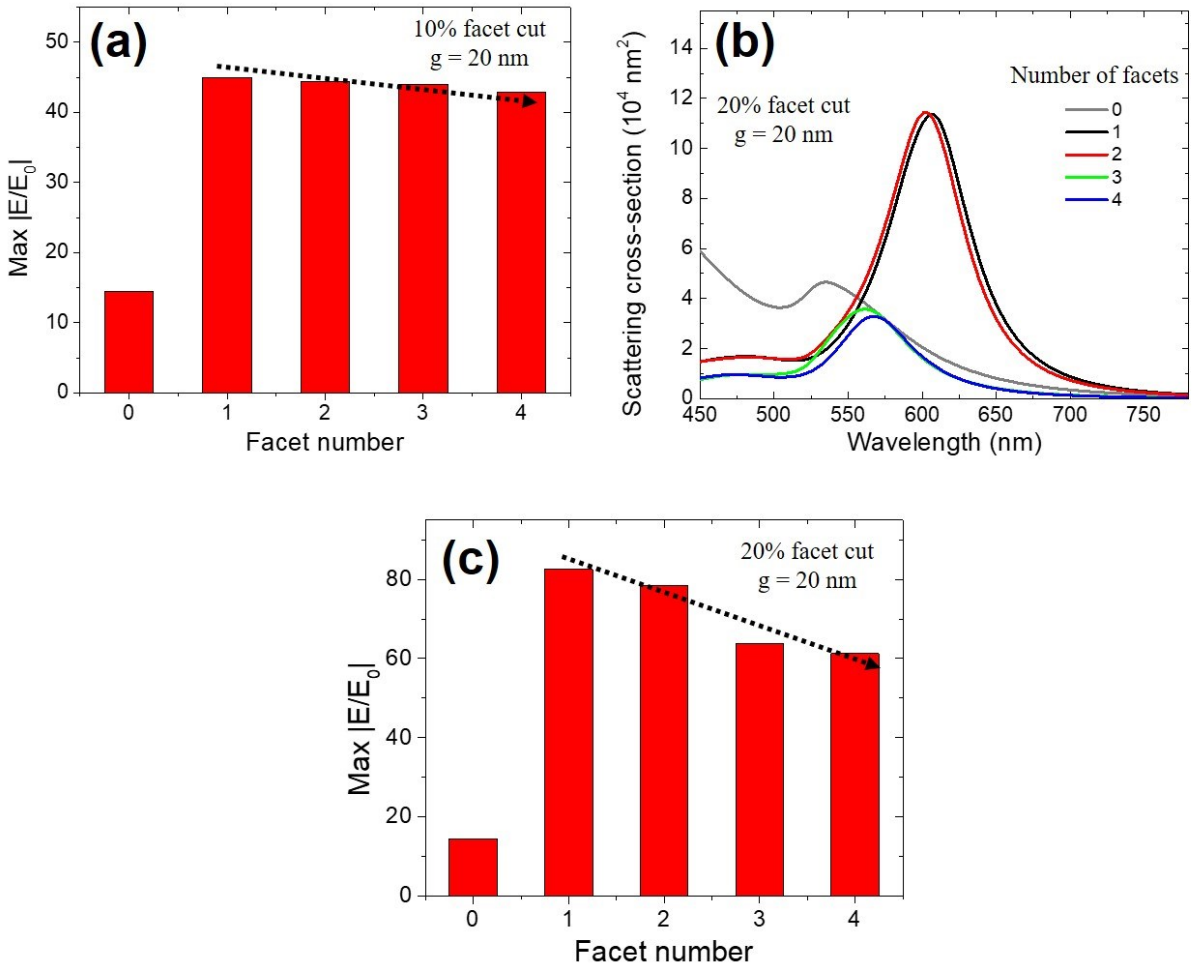

Figure S3. (a) The geometrical conditions were the same as those described in the Main text Fig. 1. The maximum obtainable near-field enhancement as a function of the facet number in the NPOM design (facet cut 10%). Scattering cross-section (b) and maximum near-field enhancement number (c) for an NPOM with a 20% facet cut. A rapid decrease in $|E/E_0|$ was observed as the facet cut depth was increased. Based on these factors, a single facet NPOM design was determined to be optimal.

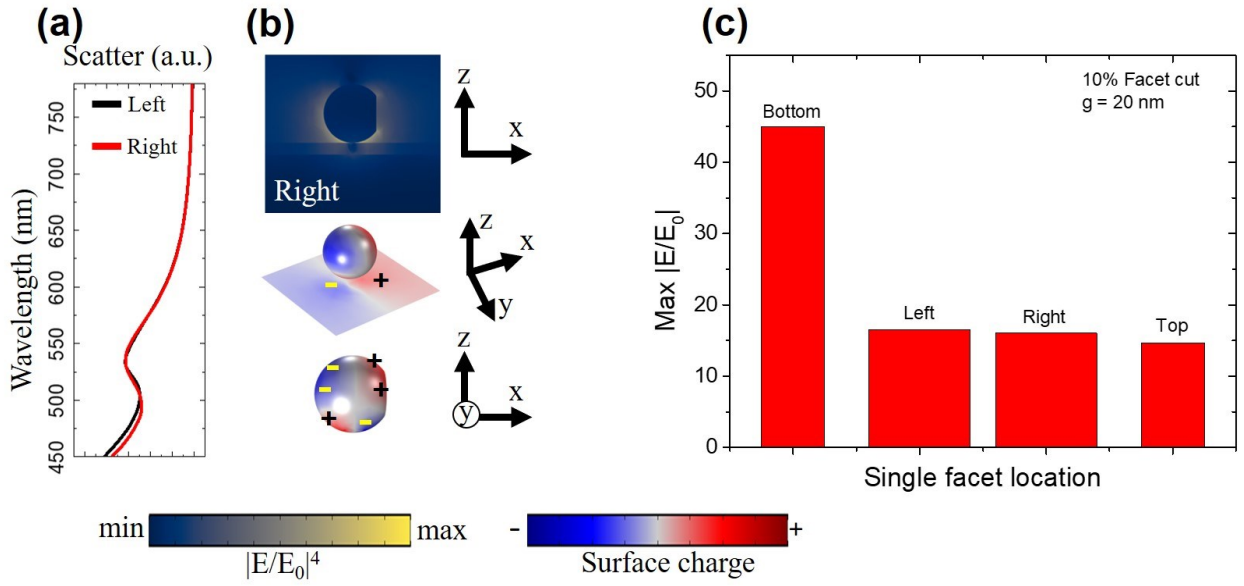

Figure S4. (a) Scattering spectra for a single-faceted NPOM positioned at left and right. (b) Cross-sectional XZ electric field amplitude profile and 3D SCDM for the single-faceted NPOM positioned to the right displaying properties similar to those of the single-faceted NPOM positioned to the left. (c) Maximum near-field enhancement numbers for different positions of the single facet in the NPOM.

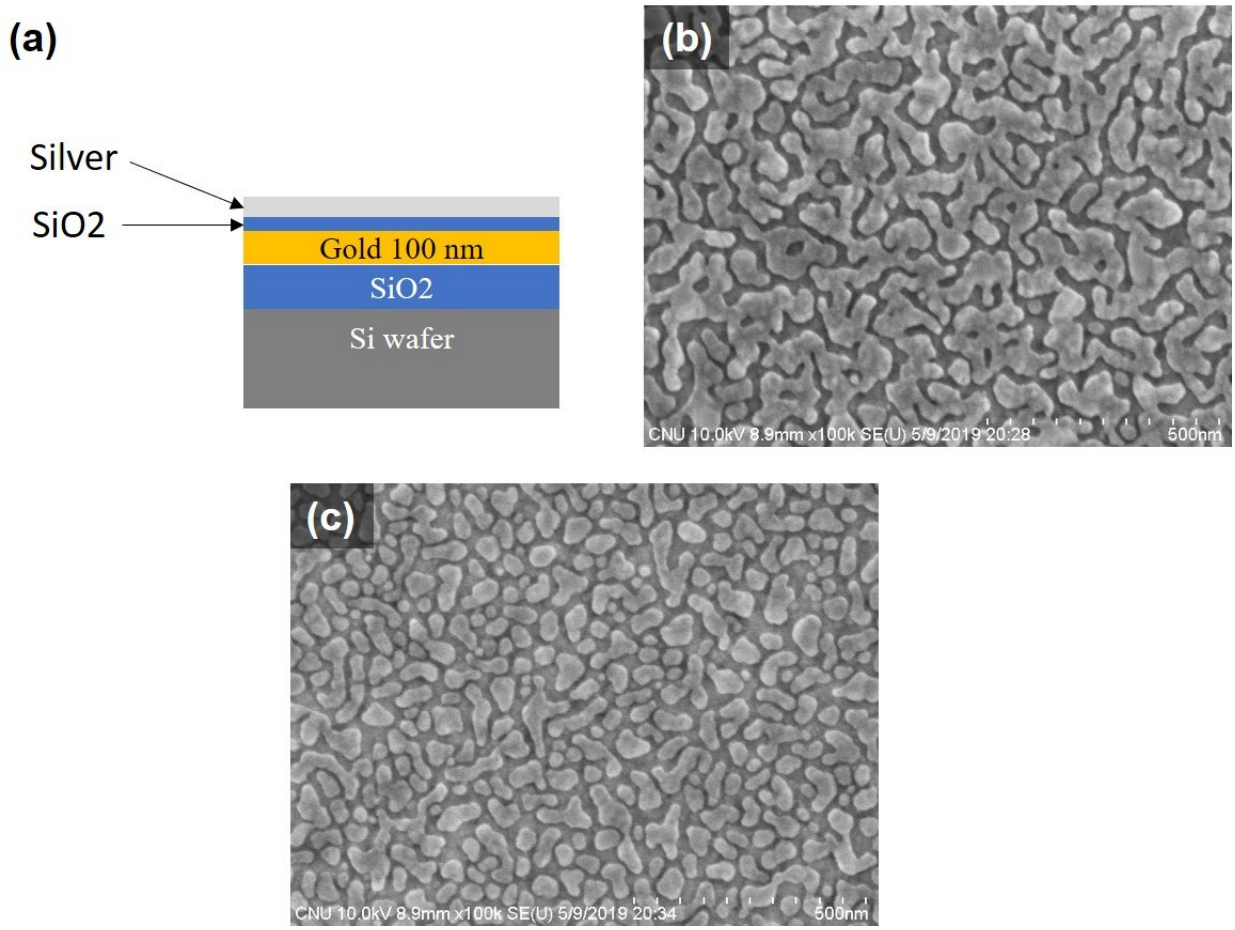

Figure S5. Characterization of the silver thin film deposited onto the silicon dioxide-coated gold substrate. (a) The structure used in this work. SEM images of the silver thin films deposited with thicknesses of (b) 11.5 nm and (c) 9 nm.

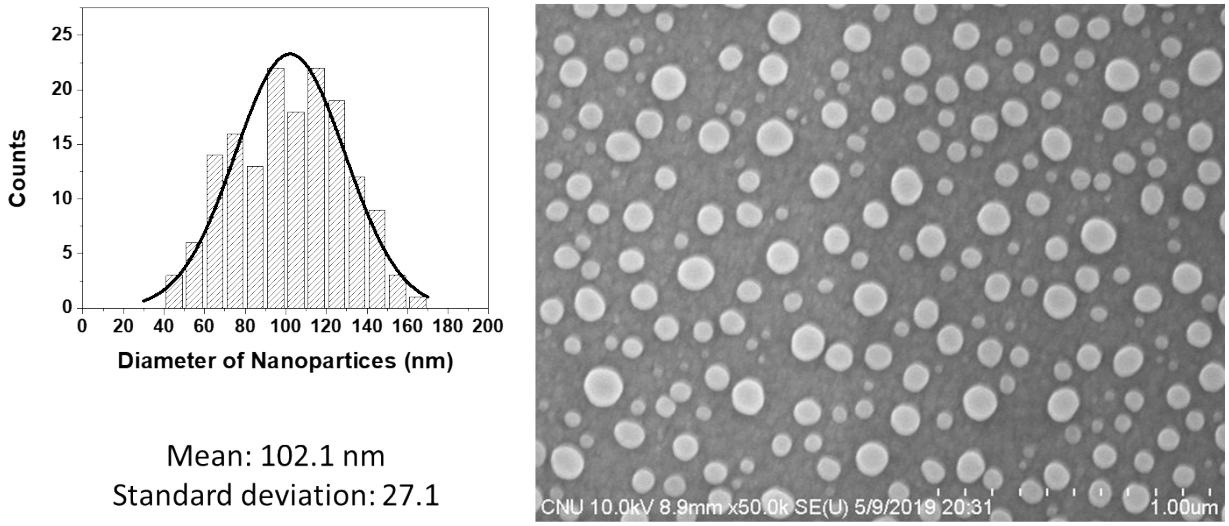

Figure S6. SEM image and size distribution of the dewetted nanoparticles, prepared using an 11.5 nm silver film.

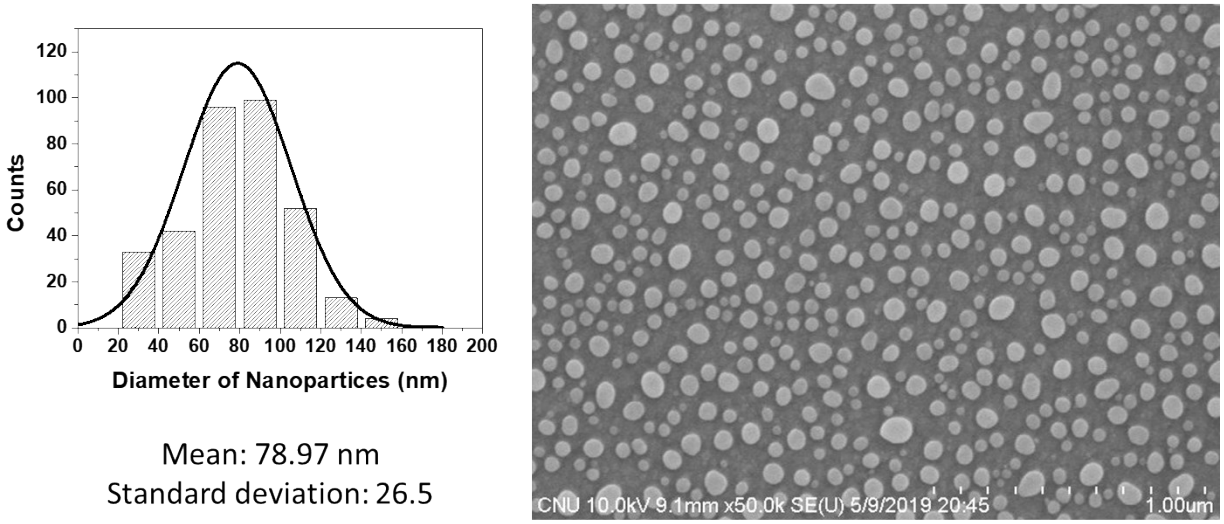

Figure S7. SEM image and size distribution of the dewetted nanoparticles, using a 9 nm silver film.

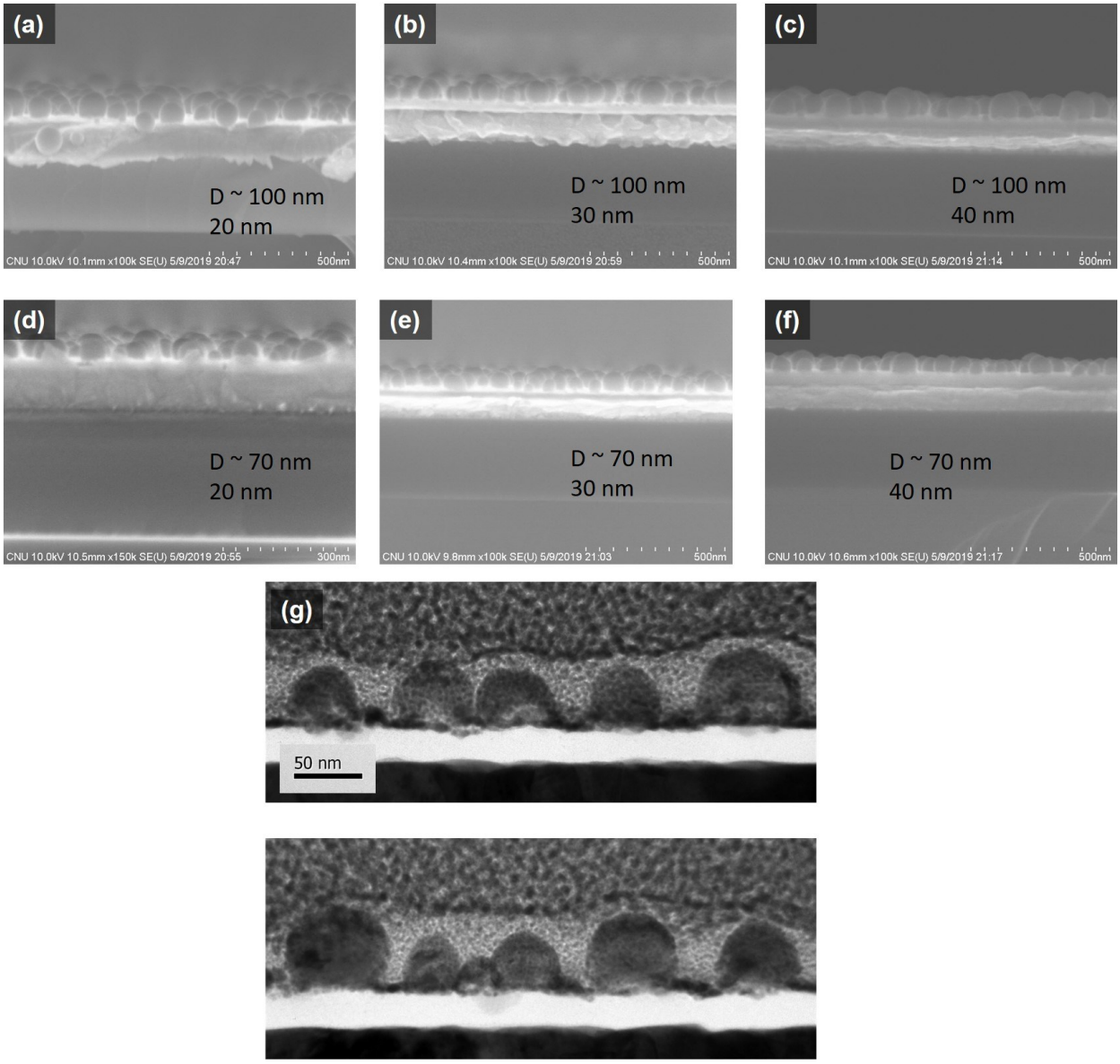

Figure S8. Cross-sectional SEM images of 100 nm single bottom-faceted nanoparticles on (a) 20 nm, (b) 30 nm, and (c) 40 nm silicon dioxide films on gold substrates. SEM images of 70 nm single bottom-faceted nanoparticles on (d) 20 nm, (e) 30 nm, and (f) 40 nm films. (g) Cross sectional TEM images of SB-FNPOMs on 30 nm SiO_2 film/gold mirror.

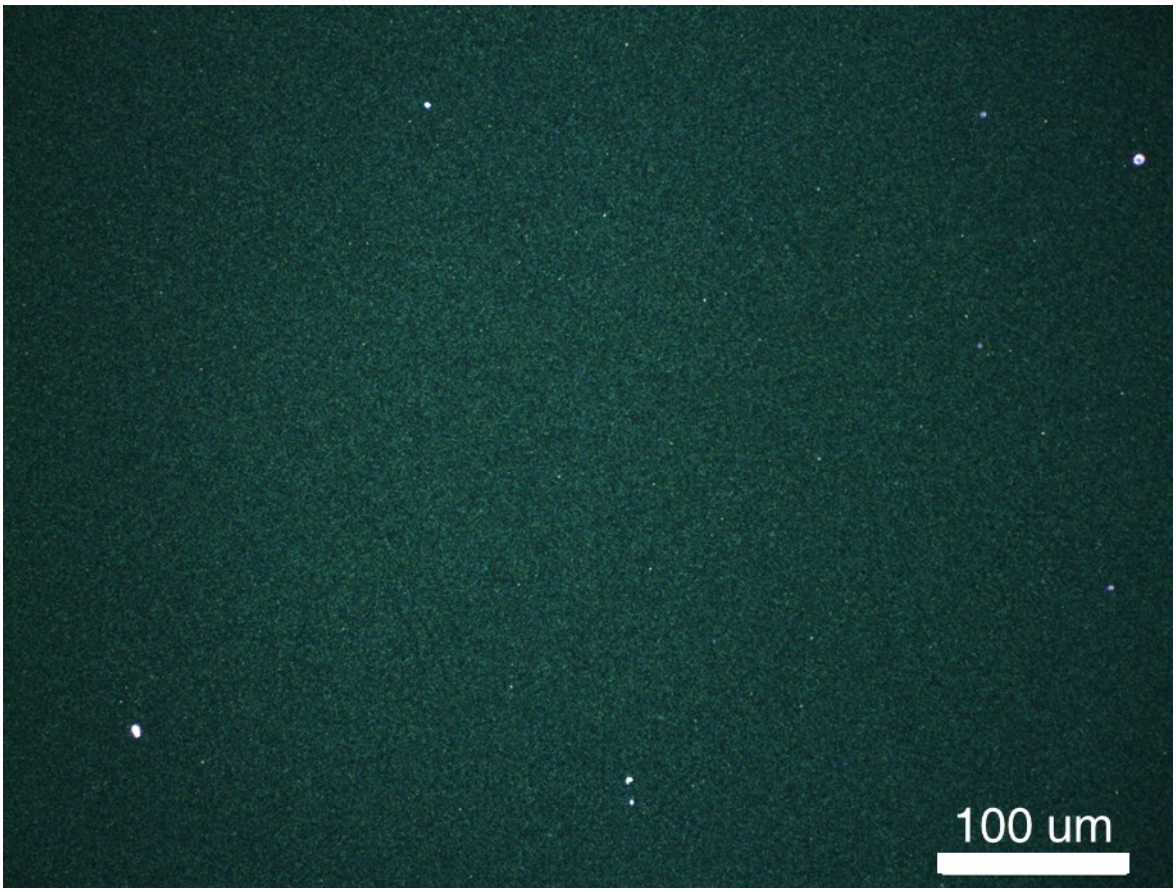

Figure S9. Dark-field microscopy image of single bottom-faceted nanoparticles on a metallic film, taken using a 20X objective.

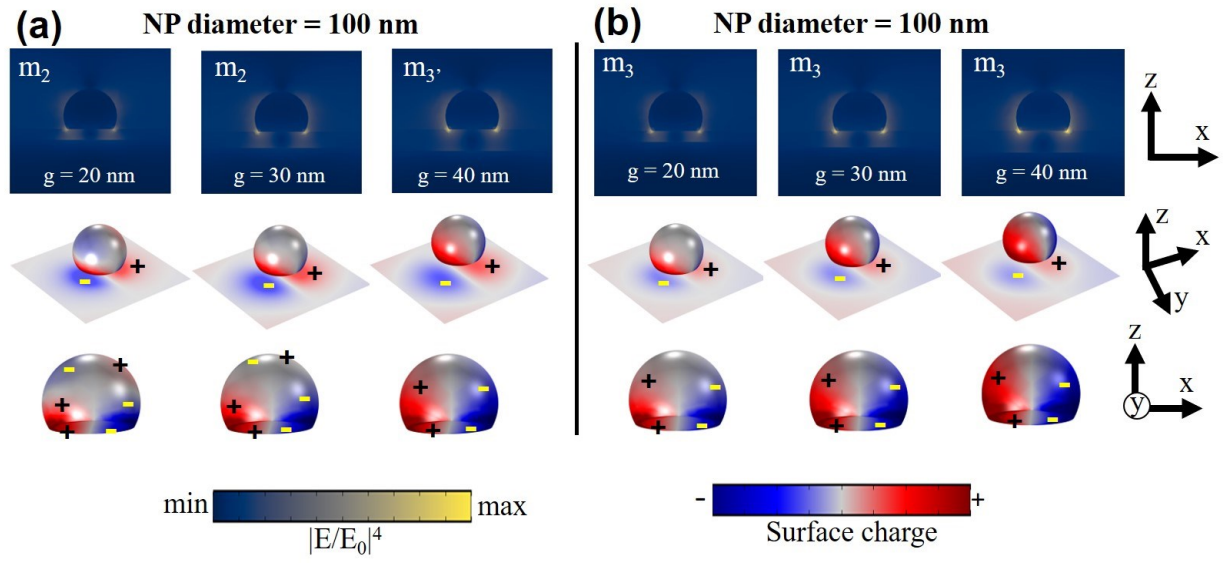

Figure S10. Cross-sectional XZ electric field amplitude profiles and 3D SCDM data obtained from a single bottom–FNPOM for an NP diameter of 100 nm at the (a) m_2 and (b) m_3 positions.

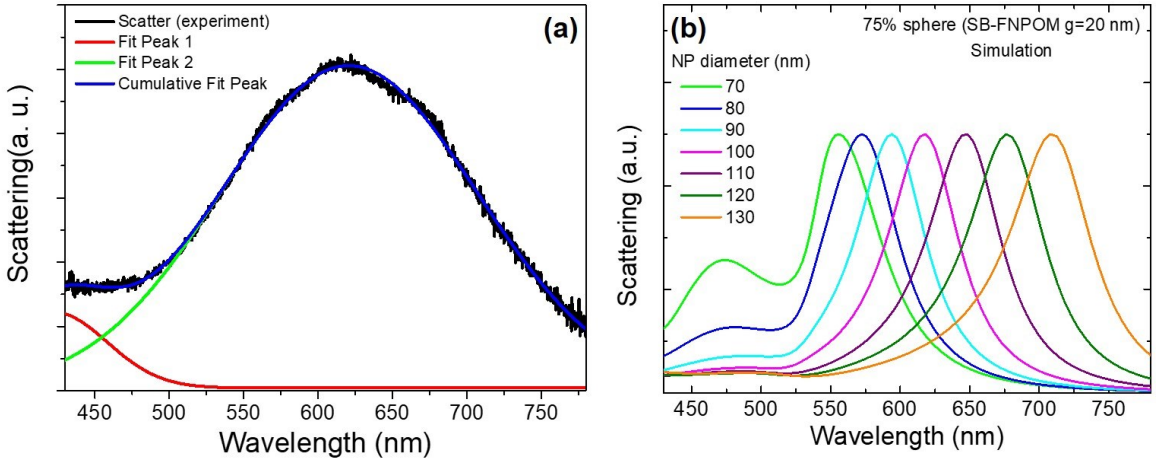

Figure S11. (a) Gaussian fitting of experimental scattering data. Clear distinguishability of gap (fit peak 2) and NP (fit peak 1) modes can be seen. (b) The simulated size distribution scattering spectra of the 75% SB–FNPOM nanostructures prepared with different NP diameters (70–130 nm), fit very well with the experimental results.

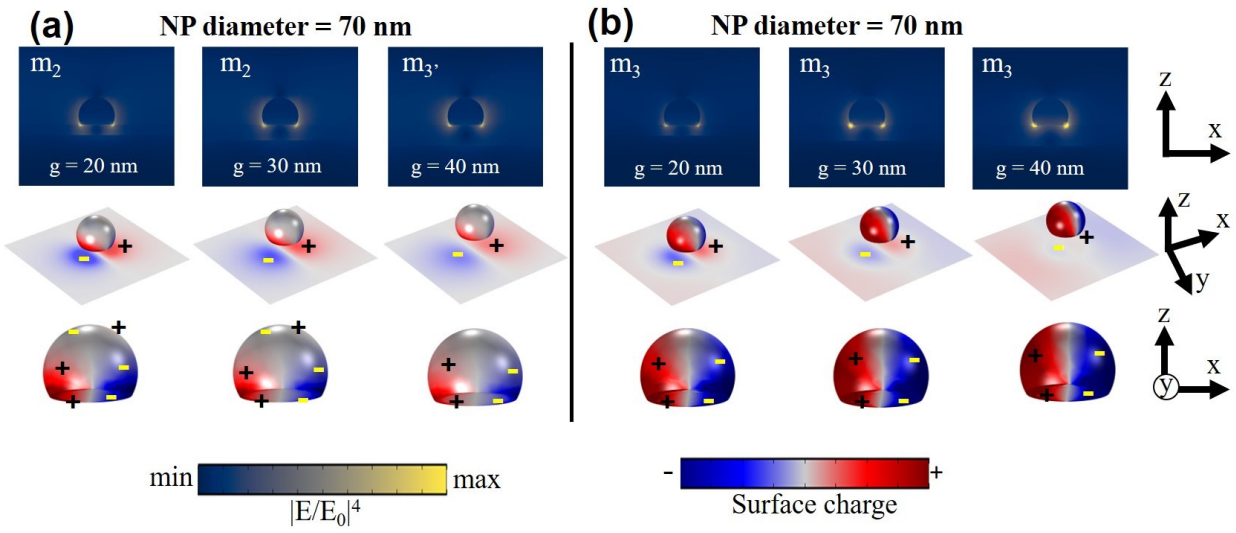

Figure S12. Cross-sectional XZ electric field amplitude profiles and 3D SCDM data obtained from a single bottom–FNPOM for a NP diameter of 70 nm at the (a) m_2 and (b) m_3 positions.

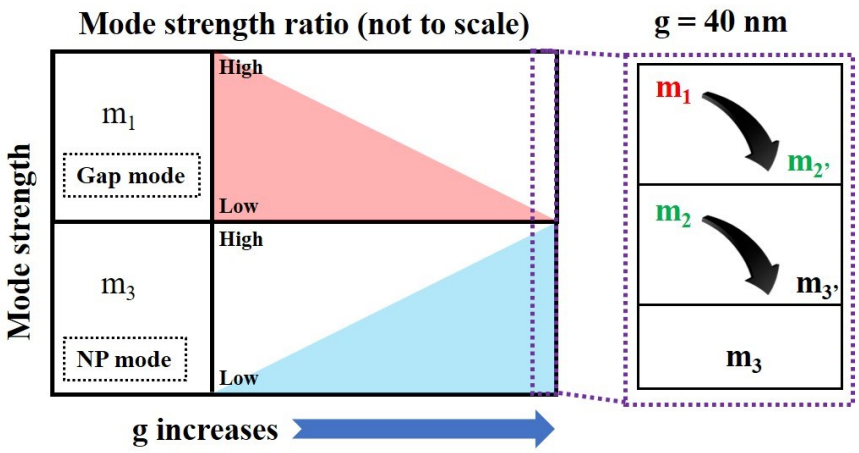

Figure S13. Ratio and influence of the mode strength as a function of the gap size g. At smaller g sizes, the influence of the gap mode was dominant and deteriorated as g increased. At g = 40 nm, the transformation of modes was observed (m_1 → $m_{2'}$; m_2 → $m_{3'}$).

Facet #	λ position of m_1 (nm)	λ position of m_2 (nm)		λ position of m_3 (nm)
1	572	509		456
2	572	509		456
3	566	504		456
4	572	506		456
0	-	534 (i)	504 (ii)	456

Table 1. Wavelength positions of m_1, m_2, and m_3 and the respective 3D SCDM and cross-sectional XZ, XY electric field amplitude profiles, as reported in the Main text Fig. 1, ESI Figs. S1 and S2.

g (nm)	λ position of m_1 (nm)	λ position of m_2 (nm)	λ position of m_3 (nm)
NP diameter = 100 nm			
20	617	512	482
30	597	512	482
40	589 ($m_{2'}$)	508 ($m_{3'}$)	482
NP diameter = 70 nm			
20	556	502	455
30	546	502	441
40	540($m_{2'}$)	500 ($m_{3'}$)	439

Table 2. Wavelength positions of m_1, m_2, and m_3 for the simulated 3D SCDM and cross-sectional XZ electric field amplitude profiles, as reported in the Main text Fig. 6, ESI Figs. S10 and S11.

Sphere D %	Facet length (nm)	
	D = 100 nm	D = 70 nm
100% (perfect sphere)	0	0
90%	~ 60.1	--
80%	~ 80.2	--
75%	~ 87.3	~ 60.8
70%	~ 92.3	--
60%	~ 97.7	--
50%	100	70

Table 3. Sphere D % and respective facet length details for NP D = 100 nm and 70 nm.